

Indian Institute of Technology Roorkee

Segregation of granular material in a rotating cylinder

by

Shivam Parashar

A thesis submitted in partial fulfillment for the
degree of Bachelor of Technology

under the supervision of
Dr. Anshu Anand
Department of Chemical Engineering

April 2018

Department of Chemical Engineering

INDIAN INSTITUTE OF TECHNOLOGY ROORKEE

Certificate

*This is to certify that the work contained in this thesis entitled “**Segregation of granular particles in a rotating cylinder**” is a bonafide work of **Shivam Parashar** (**Enrollment no. 14112091**), carried out in the Department of Chemical Engineering, Indian Institute of Technology Roorkee under my supervision and that it has not been submitted elsewhere for a degree.*

Supervisor: **Dr. Anshu Anand**

April, 2018
Roorkee.
Uttarakhand.

Assistant Professor,
Department of Chemical Engineering,
Indian Institute of Technology Roorkee,

“Ideas are cheap. Ideas are easy. Ideas are common. Everybody has ideas. Ideas are highly, highly overvalued. Execution is all that matters.”

Casey Neistat

Indian Institute of Technology Roorkee

Abstract

Dr. Anshu Anand
Department of Chemical Engineering

Bachelor of Technology

by Shivam Parashar

In this work, we have investigated segregation of granular particles inside a horizontally rotating cylinder using open source software package LIGGGHTS. In the first part of this thesis, we have described radial and axial segregation for spherical particles. We have measured degree of segregation and studied how the segregation pattern evolves with time. In the later half, we have investigated effect of particle shape on the degree of segregation. Specifically taking all combinations of prolate and oblate spheroids, their size segregation was analyzed. It was found that segregation is more pronounced for prolate-prolate mixture as compared to oblate-oblate mixture.

Acknowledgements

I am glad to express my profound gratitude to Dr. Anshu Anand, being my thesis supervisor for his help in guiding me in the course of work. I appreciate all his contributions of time and ideas to make the results of this project productive.

The members of the Particle Technology group have contributed immensely in developing my skills as a researcher. Within the group, I have had the pleasure to work with Rahul and Lipsa. I thank them for their constant support.

In the end, I would like to thank my family for raising me with an interest in science. I also thank them for supporting me in all my pursuits.

Contents

Abstract	iii
Acknowledgements	iv
List of Figures	vii
List of Tables	ix
Symbols	x
1 Introduction	1
1.1 What are Granular particles?	1
1.2 Motivation	1
1.2.1 Mixing vs segregation	1
1.2.2 Complex Behavior of Granular Materials	2
1.3 Approach of study	2
1.3.1 Discrete Element Method (DEM)	2
1.3.2 LIGGGHTS	3
1.3.3 Visualization Tools and Post Processing	4
2 Background theory	5
2.1 Discrete Element Method	5
2.1.1 Calculation Cycle	7
2.2 Radial Segregation	7
2.3 Axial Segregation	8
2.3.1 Cause of Axial Segregation	8
2.4 Implementation of Non-spherical Particles in DEM	9
2.4.1 Superquadrics	10
2.4.2 Ellipsoids and Tensors	10
2.4.3 Transformation of axes	12
3 Simulations	15
3.1 Run A: Radial Segregation of Spherical Particles	15
3.2 Run B: Axial Segregation of Spherical Particles	16
3.3 Run C: Segregation of Non-spherical Particles	16
3.3.1 Prolate - prolate	17
3.3.2 Oblate - Oblate	17

3.3.3	Small Prolate - Big Oblate	18
3.3.4	Small Oblate - Big Prolate	18
4	Results and Discussion	19
4.1	Run A: Radial segregation for binary mixture of spherical particles	19
4.2	Run B: Axial segregation for binary mixture of spherical particles	19
4.3	Run C: Segregation in Non-spherical particle mixture	22
4.3.1	Prolate-prolate Mixture	23
4.3.2	Oblate-oblate Mixture	25
4.3.3	Small-prolate Big-oblate Mixture	25
5	Conclusions	28
5.1	Outlook	28
	Bibliography	30

List of Figures

2.1	A schematic of the Hertz-Mindlin granular flow model. The collision forces are modeled as the sum of spring and deshpot forces in both the normal and tangential direction.	6
2.2	Snapshots depicting the state of the partially cylinder after certain rotations. A radial core of smaller particle is evident. (Source -M.M.H.D. Arntz et al.(2008) AIChE Journal, 54: 3133-3146)	8
2.3	Different view of axial segregation of granular particles inside a horizontally rotating drum. (Source -M.M.H.D. et al. (2008) AIChE Journal, 54: 3133-3146)	9
2.4	The figure show the different types of Superquadrics shapes obtained by just varying the parameters such as (a, b, c, n_1, n_2) in the equation.	10
2.5	Examples of prolate and oblate ellipsoids	11
2.6	Principal axis of the ellipsoid on the left are aligned with the coordinate axis, while for the ellipsoid on the right, new axis can be defined such that those axis will align perfectly along its principal axis.	13
2.7	Rotation of the initial axis by an angle θ counterclockwise along the z-axis results in the transformation of the coordinates in the new axis.	13
4.1	Radial view of simulation at $t = 1$ s and at $t = 20$ s	19
4.2	(a) and (b) are initial state while (c) and (d) are the state of the system after 125 rotations. In the final state, bands are pure with no radial core of small particles.	20
4.3	Segregation ratio is plotted against cylinder revolutions. Segregation ratio is defined such that for pure axial band, it becomes 1 and for a completely mixed state, its value is 0.	20
4.4	Space time plot representing mass fraction of large particles along the axial length.	21
4.5	Space time plot depicting total mass variation along axial length and with time.	21
4.6	Graph of angle of repose of the bed vs simulation time, plotted for both particles of different radii.	21
4.7	Segregation ratio for granular mixtures plotted against simulation time. .	23
4.8	Prolate-prolate: Initial and final snapshot at $t = 1$ s and $t = 34$ s respectively.	23
4.9	Prolate-prolate: Concentration vs simulation time for smaller and larger particles respectively	24
4.10	Prolate-prolate: Distribution of smaller and larger particles in the radial direction repectively	24
4.11	Oblate-oblate: Initial and final snapshot at $t = 1$ s and $t = 34$ s respectively.	25

4.12	Oblate-oblate: Concentration vs simulation time for smaller and larger particles respectively	25
4.13	Oblate-oblate: Distribution of smaller and larger particles in the radial direction repectively	26
4.14	Small prolate - large oblate: Initial and final snapshot at $t = 2$ s and $t = 35$ s respectively.	26
4.15	Small prolate - large oblate: Concentration vs simulation time for smaller and larger particles respectively	27
4.16	Small prolate - large oblate: Distribution of smaller and larger particles in the radial direction repectively	27

List of Tables

3.1	Properties used for radial segregation of spherical particles	15
3.2	Properties used for axial segregation of spherical particles	16
3.3	Properties used for all non-spherical particle simulations	17
3.4	Properties used for prolate-prolate mixture	17
3.5	Properties used for oblate-oblate mixture	18
3.6	Properties used for small prolate-big oblate mixture	18
3.7	Properties used for small oblate-big prolate	18

Symbols

l	Length of the cylinder	m
R	Radius of the cylinder	m
ω	Angular speed	rads ⁻¹
c_s	Number of smaller particles per uni area	m^{-2}
C_s	Number of bigger particles per uni area	m^{-2}
Δ^{seg}	Segregation ratio	Dimensionless
γ	Ratio of number of smaller to larger particles	Dimensionless
F	Force	Newton
v	Velocity	m/s
m	Mass	kg
I	Moment of Inertia	$k\text{gm}^2$
M	Torque	N/m
T	Time period of cylinder	s
g	Acceleration due to gravity	m/s^2
μ	Coefficient of friction	Dimensionless
δ	Deformation	m
ρ	Density	kg/m^3

Chapter 1

Introduction

1.1 What are Granular particles?

Granular material are a collection of discrete particles of similar kind. Since these materials are macroscopic, Newton's laws can be applied on them to predict their motions accurately. Many researchers have found that their behavior is very much different from solids. This result is interesting because each granular particles itself is a solid. It is also known that granular material also distinguishes itself from other state of matter such as liquid and gases. Therefore, many researchers and scientists consider granular material as a new form of matter. Hence it could be concluded that describing each solid particle is easy, but understanding the combined behavior of granular materials is complex allowing it to exhibit striking properties.

1.2 Motivation

1.2.1 Mixing vs segregation

The process of mixing different kinds of granular particles is a common unit-operation adopted in a chemical industry. Therefore, a large fraction of equipments in industries are blenders. The simplest type of blender is a horizontally rotating cylinder. Many industries use it for mixing the granular particles without much understanding of the phenomena. They spend millions of dollars on these equipments to produce desirable mixing. A problem faced by these industries is that under certain conditions, particles are segregated instead of getting mixed. This result is counterintuitive but has been proved by various researches both theoretically and experimentally. This segregation of particles is a problem for the industries that needs be tackled by proper design of the blenders. This can only be done by fully understanding the segregation phenomena.

Therefore, it is crucial to understand the conditions at which the segregation of granular material would take place.

1.2.2 Complex Behavior of Granular Materials

From the above discussion it is clear that granular material posses complex behavior as a whole. This can be understood by comparing the response of two different objects in relation to the granular material. Take two containers, both of them half filled with salt (a granular material) but one contains a steel nut and the other contains a thumb pin. If the container is shaken horizontally, the thumb pin would rise up but the steel nut would sink into the salt. The outcome of such an experiment exposes the complexity that is exhibited by the granular materials. Therefore, because of its importance in the chemical industry and intriguing behavior, granular mixing has been a focus of researchers across the globe from the past decade.

1.3 Approach of study

1.3.1 Discrete Element Method (DEM)

Discrete element method (DEM) is a numerical methods which is used to predict the motion of a large number of macroscopic particles. It is a particle-scale numerical method for modeling the bulk behavior of granular materials such as sand, rocks, pellets, tablets and powders. DEM can be used to get insight into the particle flow dynamics. Another advantage DEM caters is its ability to model moving and periodic boundaries. The knowledge is then applied to design more efficient equipment (such as rotating cylinder, fluidized bed and hopper), thus improving process efficiency and product quality.

In the past 30-40 years, a lot of researchers had focussed on 2-dimensional systems because of the unavailability of enough computational resources during that period of time. But with the advent of the best supercomputers and clusters, in the last decade it has been made possible to simulate 3-dimensional systems that too on a large scale. These simulations have always backed up the researchers with their experimental findings. Through simulations it has been made possible to tackle some typical experimental obstacles and to get a complete understanding of the phenomena.

In our study, we have employed DEM simulations to understand the segregation behavior of spherical and non-spherical particles inside a rotating cylinder using LIGGGHTS. DEM simulation employs the lagrangian approach which makes mathematics simpler than the classical newtonian approach. The lagrangian is defined as :

$$L = T - V \quad (1.1)$$

where T is the kinetic energy and V is the potential energy. The Euler-Lagrange Equation (Second kind) is given by:

$$\frac{\partial L}{\partial q} = \frac{d}{dt} \frac{\partial L}{\partial \dot{q}} \quad (1.2)$$

where q is a vector present in the configuration space.

Newton's second law of motion for translational motion can be written as:

$$m_i \frac{dv_i}{dt} = \sum_{j=1}^k F_{c,ij} + m_i g \quad (1.3)$$

where m_i is the mass of the i^{th} particle, v_i is the linear velocity of the i^{th} particle. $F_{c,ij}$ is the collision force acting between particle i and particle j.

Newton's second law of motion for rotational motion can be written as:

$$I_i \frac{d\omega_i}{dt} = \sum_{j=1}^k M_{ij} \quad (1.4)$$

where I_i denotes the moment of inertia of the i^{th} particle; ω_i denotes the angular velocity of the i^{th} particle. g denotes acceleration due to gravity, t denotes the time, and k denotes the number of collisions. M_{ij} is the moment generated between those two colloidal particles.

1.3.2 LIGGGHTS

LIGGGHTS stands for LAMMPS improved for general granular and granular heat transfer simulations. LAMMPS is one of the most popular and widely used molecular dynamics simulator.

A typical LIGGGHTS input script consists of four parts:

1. Initialization - It involves setting the parameters such as atom style, types of boundaries (moving, fixed or periodic), units etc.
2. Atom definition - It consists of creating the particles by defining the region in which the particles are inserted.
3. Settings - It involves defining all the properties of the atoms and the granular wall such as youngs modulus, poissons ratio, coefficient of restitution, coefficient of friction. This section also defines the size of a timestep.
4. Running a simulation - It simply launches the simulation based on what is defined in the above three sections.

An additional **STL** (stereolithography) file is also needed to describe the 3-dimensional geometry of the walls that encloses the granular particles.

1.3.3 Visualization Tools and Post Processing

Once the input script is complete and the system is described fully with appropriate STL files, LIGGGHTS simulations can be launched. Output files constitutes the position and velocity of each particle generated at every timestep (as specified in the input script). The so generated position data was converted to a snapshots with the help of **Paraview**. The data containing particle coordinates as a function of time were used to calculate useful quantities such as segregation ratio, particle distributions, angle of repose etc. This was done by writting several scripts in **Python** and **Bash**. To generate space-time plots and graphs of above mentioned quantities, **Xmgrace** and **Gnuplot** were used.

Chapter 2

Background theory

2.1 Discrete Element Method

In LIGGGHTS, the DEM code is implemented to a new HertzMindlin granular contact model (see fig. 2.1). In this contact model, the normal and tangential collision forces are approximated as the sum of the spring force and the deshpot force. The total collision force between the particles is given by:

$$\vec{F} = \vec{F}_n + \vec{F}_t \quad (2.1)$$

where \vec{F}_n is a normal force acting between two particles and F_t is the tangential force. \vec{F}_n is given by:

$$\vec{F}_n = K_n \delta_{n,ij} - \gamma_n v_{n,ij} \quad (2.2)$$

where K_n is a wall stiffness coefficient in the normal direction, γ_n is a viscoelastic damping constant in the normal direction, $\delta_{n,ij}$ is the overlap distance between the two colliding particles, and $v_{n,ij}$ is the normal component of the relative velocity between those two particles.

Collision force in the tangential direction F_t is given by:

$$\vec{F}_t = K_t \delta_{t,ij} - \gamma_t v_{t,ij} \quad (2.3)$$

where K_t is a wall stiffness coefficient in the tangential direction, γ_t is a viscoelastic damping constant for tangential direction $\delta_{t,ij}$ is the tangential overlap distance of two grains, and $v_{t,ij}$ is the tangential component of the relative velocity between those two particles.

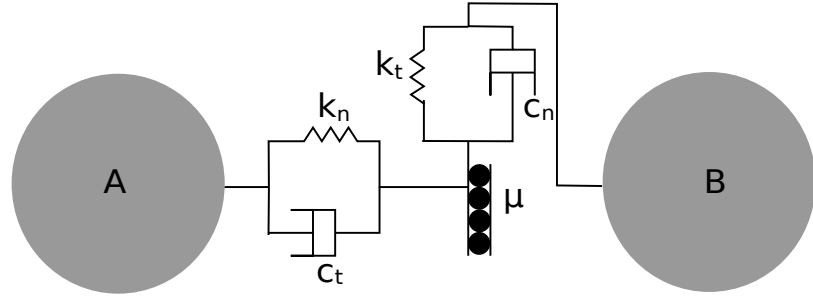


FIGURE 2.1: A schematic of the Hertz-Mindlin granular flow model. The collision forces are modeled as the sum of spring and deshpot forces in both the normal and tangential direction.

For Hertz-mindlin model, we measure $K_n, K_t, \gamma_n, \gamma_t$ coefficients as follows:

$$K_n = \frac{4}{3} Y^* \sqrt{R^* \delta_n} \quad (2.4)$$

$$\gamma_n = -2\sqrt{5/6}\beta\sqrt{S_n m^*} \quad (2.5)$$

$$K_t = 8G^* \sqrt{R^* \delta_n} \quad (2.6)$$

$$\gamma_t = -2\sqrt{5/6}\beta\sqrt{S_t m^*} \quad (2.7)$$

For two granular particles in contact with each other, the following equation can be written:

$$S_n = 2Y^* \sqrt{R^* \delta_n} \quad (2.8)$$

$$S_t = 8G^* \sqrt{R^* \delta_n} \quad (2.9)$$

$$\beta = \frac{\ln(e)}{\sqrt{\ln^2(e) + \pi^2}} \quad (2.10)$$

$$\frac{1}{Y^*} = \frac{(1 - \vartheta_1^2)}{Y_1} + \frac{(1 - \vartheta_2^2)}{Y_2} \quad (2.11)$$

$$\frac{1}{G^*} = \frac{2(2 + \vartheta_1)}{Y_1} + \frac{2(2 + \vartheta_2)}{Y_2} \quad (2.12)$$

$$\frac{1}{R^*} = \frac{1}{R_1} + \frac{1}{R_2} \quad (2.13)$$

$$\frac{1}{m^*} = \frac{1}{m_1} + \frac{1}{m_2} \quad (2.14)$$

where G is the shear modulus, Y is the Young's modulus, ϑ is the poisson ratio, e is the coefficient of restitution, m is the mass and R is the radius of a particle. The subscript 1 and 2 stands for two particles in contact.

2.1.1 Calculation Cycle

In DEM, same algorithms repeats itself after each time-step. Calculation from previous time-steps are used for computations at current timesteps. If a large number of sphere collides among themselves, then DEM performs two iterations for each time step- in first step, collision forces are calculated depending upon the deformation caused on each particle. In the second step, the coordinates of each particle are revised depending upon the forces acting on that particle. Since during the collision, non-impulsive forces such as gravity can be neglected therefore, contact forces plays an important role in the first step. Application of Newton's laws becomes crucial in the second step. Within a single timestep, the impulsive collision forces can be assumed to be constant, therefore, from Newton's laws the new position of the particle can be obtained. The algorithm of DEM repeats this procedure for all the particles present in the system.

2.2 Radial Segregation

When the cylinder is operated in the avalanching flow regimes, there is a strong tendency of small sized particle to percolate through the bed of bigger particles and accumulate close to center of the cylinder. This segregation is termed as radial. This type of segregation takes place within first few rotations of the cylinder. Inverted segregation also exist which is characterized by a core of bigger particles surrounded by small sized

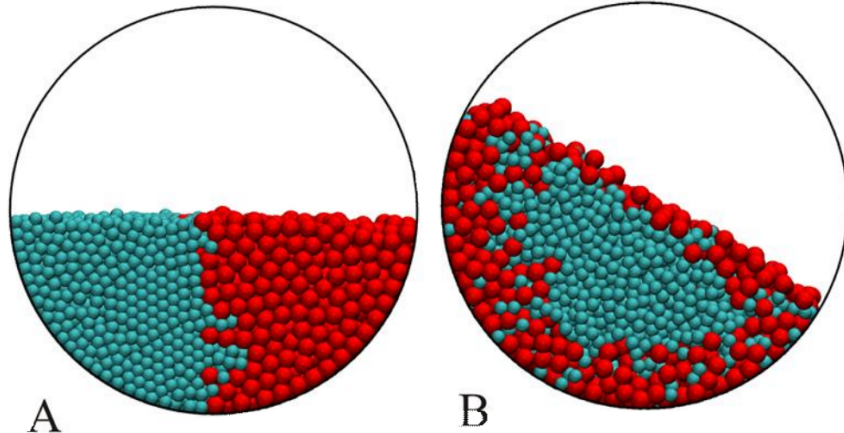


FIGURE 2.2: Snapshots depicting the state of the partially cylinder after certain rotations. A radial core of smaller particle is evident. (Source -M.M.H.D. Arntz et al.(2008) AIChE Journal, 54: 3133-3146)

granules. This generally takes place at large rotational speeds of the cylinder. Therefore, it could be concluded that at lower rotational speed of the cylinder, percolation of small sized granules dominates whereas at higher angular speed, percolation is negligible which results in a core of bigger particles.

2.3 Axial Segregation

If the cylinder is allowed to rotate continuously, even after the radial segregation pattern has formed, then under certain conditions, the core of denser particles becomes unstable, and it leads to the formation of alternate pure bands of each type of particle. This phenomenon is known as axial segregation. (see fig. 2.3). Many researchers understand the phenomenon of axial segregation as a fluctuation in the radial segregated core. In most of the previous experimental studies, radial core of smaller particles was retained as the band were forming, but in our simulations we observed that the radial core was absent and therefore each band was pure.

2.3.1 Cause of Axial Segregation

Angle of repose for granular particles is defined as the angle that is made by the surface of the bed when the material is rotated in a cylinder. Many researchers claim that a difference in angle of repose is necessary for axial segregation to take place. Many researchers tried to explain the mechanism of axial segregation but a complete explanation of the phenomenon was given by Bridgwater et al. (1969) as follows. Since the side walls

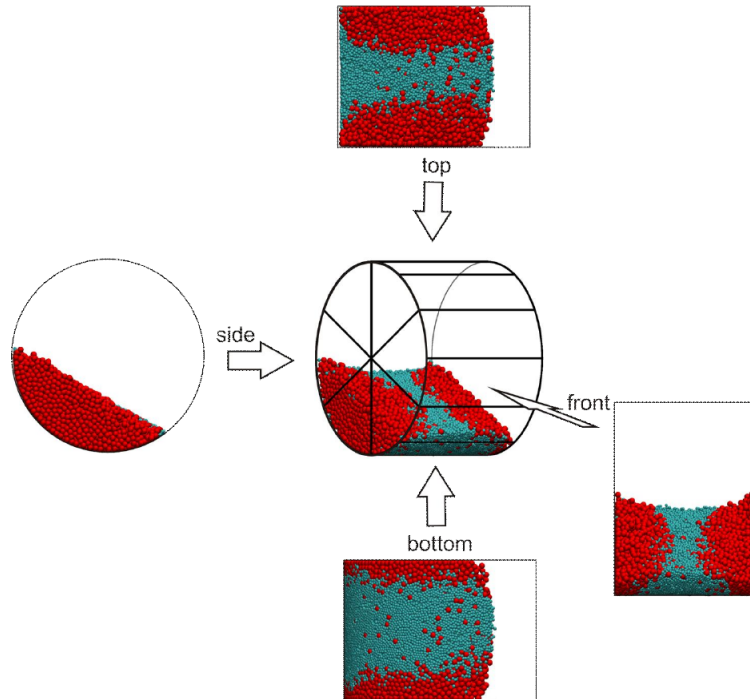


FIGURE 2.3: Different view of axial segregation of granular particles inside a horizontally rotating drum. (Source -M.M.H.D. et al. (2008) AIChE Journal, 54: 3133-3146)

of the cylinder are not frictionless, the angle of repose for both particles near the side walls would be greater than at the middle of the cylinder. Therefore both types of particles could be seen as bouncing a lot near those walls. Larger particles have a tendency to settle to lower points on the slope because of their mass. Therefore, more and more large particles accumulate in the lowest point of the bed. This in fact results in a relatively higher concentration of smaller particles just away from the wall. But since smaller particles have an angle of repose higher than the larger particles, it leads to further reduction in the concentration of smaller particles close to the wall. This happens at both side plates of the cylinder and eventually results in the segregation band near the walls. Band away from the side walls are formed a while after formation of the ends near the wall. It is assumed that statistical fluctuations leads to the formation of bands near the center of the cylinder.

2.4 Implementation of Non-spherical Particles in DEM

A lot of studies using DEM are performed on spherical particles because of the simplicity in its implementation. Simulation of non-spherical particles is challenging as the orientation of particle also becomes important and therefore contact detection becomes difficult. Realistic representation of shape in DEM remains a challenge for the researchers. Only recently it has been possible to introduce a class of 3-d shapes known

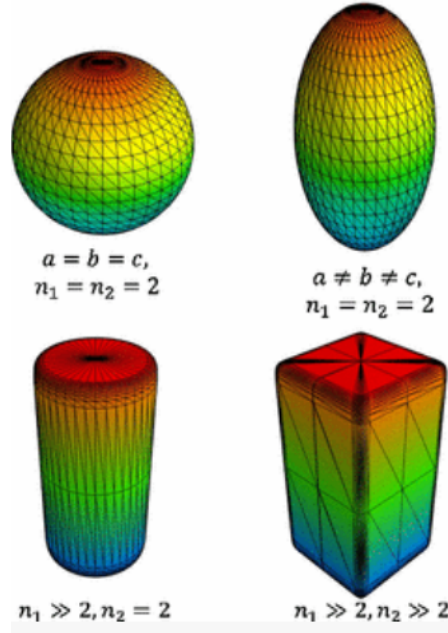


FIGURE 2.4: The figure show the different types of Superquadrics shapes obtained by just varying the parameters such as (a, b, c, n_1, n_2) in the equation.

as Superquadrics. This class of objects can represent some basic shapes like ellipsoid, cylinder and cuboids. But still, it has not been possible to introduce a general shaped particle in DEM. Nevertheless, the general equation of superquadrics can be written as:

$$f(x) = \left(\left| \frac{x}{a} \right|^{n_2} + \left| \frac{y}{b} \right|^{n_2} \right)^{\frac{n_1}{n_2}} + \left| \frac{z}{c} \right|^{n_1} - 1 \quad (2.15)$$

2.4.1 Superquadrics

a, b, c are the lengths along its principle axes. From fig. 2.4 it is clear that the superquadric equation is able to decribe four common shapes such as sphere, ellipsoid, cylinder and cuboid by the variation in the five parameters ((a, b, c, n_1, n_2)). The disadvantage of using superquadrics is that it is not able to describe shapes such as cones, pyramids and many others. Another disadvantage is the huge increase in the computation time as compared to a similar simulation launched for spherical particles. The computation times also drastically increases with the blockiness parameters n_1 and n_2 .

2.4.2 Ellipsoids and Tensors

The equation of ellipsoid with its center at the origin of the coordinate axes and the principal axes aligned in the direction of the coordinate axes can be written as:

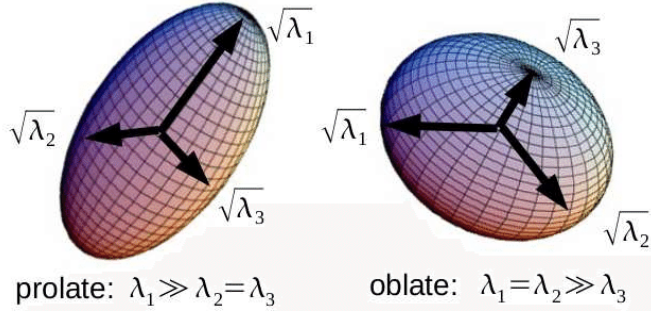


FIGURE 2.5: Examples of prolate and oblate ellipsoids

$$ax^2 + by^2 + cz^2 = 1 \quad (2.16)$$

where $1/a_1, 1/b_1$ and $1/c_1$ are the lengths of the semi-axes of the ellipsoid along the x, y and z axes, respectively. If any two semi-axes are equal , the same equation will describe a spheroid. In case all the semi-axes lengths are equal i.e. if $a = b = c$ same equation will describe a sphere.

For a generally oriented ellipsoid, such that its center still coincides with the origin of the coordinate axis (see Fig. 2.6), the equation can be written as:

$$ax^2 + by^2 + cz^2 + dxy + eyz + fxz = 1 \quad (2.17)$$

The equation does not contains any linear term in x, y or z which implies that the center of this ellipse is at the origin (just to check). The eq. 2.17 contains six parameters that would combiney determine the length of the semi-axes along each direction and its orientation. We can write eq. 2.17 in the matrix form as:

$$\begin{bmatrix} x & y & z \end{bmatrix} \begin{bmatrix} a & f & e \\ f & b & d \\ e & d & c \end{bmatrix} \begin{bmatrix} x \\ y \\ z \end{bmatrix} = 1 \quad (2.18)$$

Simply multiplying the matrix terms in eq. 2.18 would result back into eq. 2.17. Eq. 2.18 can also be written as:

$$x_i \Phi_{ij} x_j = 1 \quad (2.19)$$

where Φ_{ij} is a symmetrical tensor and contains six different components (a, b, c, d, e, f) and is given by

$$\Phi_{ij} = \begin{bmatrix} a & f & e \\ f & b & d \\ e & d & c \end{bmatrix} \quad (2.20)$$

x_j is the position vector and x_i is its transpose. One of the interesting property of the matrix Φ_{ij} is that its eigenvalues are equal to the length of the principal axis along three directions. Moreover, the eigenvector corresponding to each eigenvalue will give the direction in which each principal axis is aligned. It is known for a diagonal matrix, that the eigenvalues are simply equal to the elements present on the diagonal. Therefore, in order to calculate the eigenvalues we transform Φ_{ij} into its diagonal form. If we see this transformation geometrically, it would result in the transformation of the equation of ellipsoid from eq. 2.17 to eq. 2.16. In other words the transformation will cause the principle axis to align in the direction of our coordinate frame:

$$\Phi_{ij} = \lambda^{(i)} \delta_{ij} \quad (2.21)$$

where $\lambda^{(i)}$ are a set of eigenvalues of the tensor Φ_i and δ_{ij} is the unit matrix of suitable dimensions. In mathematics following equation holds true for eigenvalues and eigenvectors:

$$\Phi_{ij} n_j = \lambda n_j \quad (2.22)$$

In order to calculate the eigenvalues we need to solve the equation:

$$(\Phi_{ij} - \lambda \delta_{ij}) n_j = 0 \quad (2.23)$$

There only solution is $\mathbf{n}_j = 0$, unless the determinant of the $\Phi_{ij} - \lambda \delta_{ij}$ coefficients vanishes. Since the first case is absurd, the determinant must be set to zero.

$$| \Phi_{ij} - \lambda \delta_{ij} | = 0 \quad (2.24)$$

Solving the above equation will yield three values of λ , since the equation has a degree of three. So this is how, one can obtain the length of semi axes of an ellipsoid given its general equation.

2.4.3 Transformation of axes

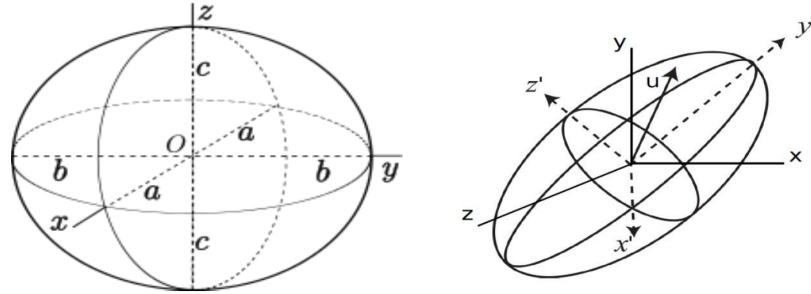


FIGURE 2.6: Principal axis of the ellipsoid on the left are aligned with the coordinate axis, while for the ellipsoid on the right, new axis can be defined such that those axis will align perfectly along its principal axis.

Let's say we have a point in our usual X-Y frame such that its coordinates are (x,y) . Suppose we rotate our coordinate axis with respect of positive z axis by angle of θ measure in the counterclockwise direction, than the point will appear on a different position as seen from X'-Y' frame. Its coordinates in this new frame would be (x',y') (refer to fig. ??). It is possible to relate the coordinates of particles in the original frame with the coordinates in the new frame of reference.

For two dimensions, the transformation for the rotation of coordinate axis about the z-axis by an angle of θ in the counterclockwise direction could be written as:

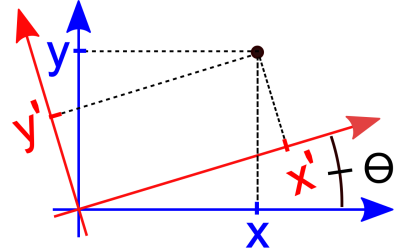


FIGURE 2.7: Rotation of the initial axis by an angle θ counterclockwise along the z-axis results in the transformation of the coordinates in the new axis.

$$\begin{bmatrix} x' \\ y' \end{bmatrix} = \begin{bmatrix} \cos(\theta) & \sin(\theta) \\ -\sin(\theta) & \cos(\theta) \end{bmatrix} \begin{bmatrix} x \\ y \end{bmatrix} \quad (2.25)$$

The most general three-dimensional rotation matrix represents a counterclockwise rotation by an angle θ about a fixed axis that lies along the unit vector \mathbf{u} . The rotation matrix operates on vectors to produce new vectors along the new coordinate axis, while keeping the vector to be fixed. In this case, the four number u_x, u_y, u_z and θ are called as the quaternions, where u_x, u_y, u_z are the components of the vector \mathbf{u} .

The general transformation equation for rotation in 3-dimensions can be written as:

$$X' = RX \quad (2.26)$$

where

$$R = \begin{bmatrix} \cos(\theta) + u_x^2(1 - \cos(\theta)) & u_x u_y (1 - \cos(\theta)) - u_z \sin(\theta) & u_x u_z (1 - \cos(\theta)) + u_y \sin(\theta) \\ u_y u_x (1 - \cos(\theta)) + u_z \sin(\theta) & \cos(\theta) + u_y^2(1 - \cos(\theta)) & u_y u_z (1 - \cos(\theta)) - u_x \sin(\theta) \\ u_z u_x (1 - \cos(\theta)) - u_y \sin(\theta) & u_z u_y (1 - \cos(\theta)) - u_z \sin(\theta) & \cos(\theta) + u_z^2(1 - \cos(\theta)) \end{bmatrix} \quad (2.27)$$

And X' and X are the coordinates of the point in their respective frame of reference. For any ellipsoidal particle, the semi-axes lengths along all the axes are known as an input. LIGGGHTS gives the orientation of the non-spherical particles in terms of quaternions which needs to be converted to a 3×3 tensor for the Paraview to visualize it. This 3×3 tensor should be in the original frame of reference. Therefore, above equation can be used to shift the axis of particle to its original frame with the help of quaternions data provided by LIGGGHTS. The eigenvalues of the original tensor are its semi-axis lengths, whereas the eigenvectors are the column vectors of the rotation matrix \mathbf{R} . Therefore, we require to find the matrix \mathbf{A} .

A diagonalizable matrix is diagonalized by a matrix of its eigenvectors. So

$$A = P \Lambda P^{-1} \quad (2.28)$$

where the eigenvectors of A would be the columns of the matrix P and Λ is a diagonal matrix whose entries are the eigenvalues of A (listed in the same order as their corresponding eigenvectors listed in P). In our case the eigenvectors are the columns of the matrix R . A python code was scripted to perform the above computation on all the particles and at each time step.

Chapter 3

Simulations

3.1 Run A: Radial Segregation of Spherical Particles

We have performed DEM simulations in three-dimensions using the open source package LIGGGHTS on a system of 24,000 particles of different sizes. We chose the inner diameter of the cylinder to be equal to $D = 0.14$ m and $l = 0.14$ m. The mass fraction of small and larger granules was kept to be 0.5. Any value of friction coefficient was not changed.

The particles were created in a well defined cylindrical region inside the drum. A fixed number particles were generated in the above defined region after every 1000 timesteps. LIGGGHTS makes it sure that no two particles are overlapping in the generation process. Once sufficient particles were generated, the system was allowed to settle for certain interval of time before the drum was rotated.

Properties	Values
Density of Sphere (kg/m^3)	2500
Young's modulus (Pa)	2.5×10^5
Poisson ratio	0.25
Coefficient of restitution	0.5
Friction between grains and inner wall	0.2
μ_{gw}	
Number of grains	24000
Diameter of grain (mm)	1.4
Timestep (s)	10^{-5}
Friction between grains μ_{gg}	0.175
Friction between grains and end-plates	0.5
μ_{gw}	

TABLE 3.1: Properties used for radial segregation of spherical particles

3.2 Run B: Axial Segregation of Spherical Particles

The run consisted of 50,000 particles, with the length of the drum = 1.6 m and diameter = 0.2 m. The coefficient of friction between all surfaces was kept same. This is done to make sure that the two kinds of particles were different by size only. Particles were generated in a manner similar to that described in run A.

Properties	Values
Density of Sphere (kg/m^3)	2,500
Young's modulus (Pa)	10^8
Poisson ratio	0.24
Coefficient of restitution	0.97
Coefficient of friction between particles and inner wall μ_{gw}	0.6
Coefficient of friction between particles μ_{gg}	0.6
Coefficient of friction between particles and end-plates μ_{gw}	0.6
Number of grains	50,000
Diameter of particles (mm)	2.4, 4.8
Mass fraction of each type of granules (respectively)	0.5 and 0.5
Timestep (s)	10^{-6}
Time period of rotation (s)	2
Dimensions of Cylinder (m)	$l = 1.6$ and $R = 0.1$

TABLE 3.2: Properties used for axial segregation of spherical particles

3.3 Run C: Segregation of Non-spherical Particles

Non-sphericity of particles often plays an important role. Earlier, non-spherical particles were simulated by approximating the geometry to a number of spheres of different sizes glued together. This approach is known as the Multisphere method for representing non-spherical particles. With the advent of fast computers, it is now possible to simulate certain shapes precisely. These codes have been recently added to the LIGGGHTS package that allows it to generate a class of 3d objects known as Superquadrics. This class can be used to generate shapes such as ellipsoids, cylinder, cuboids and cubes.

Among the non-spherical particles, we have decided to study the segregation for various combination of prolate and oblate spheroids. In each case size of both the particles are different. In all the simulations described below, total number of particles was kept to be 5,000 which is much less than that the previous simulations. The reason is that the contact detection, torque and orientation calculations makes it computationally expensive to run simulation for non-spherical particles.

Properties	Values
Density of Sphere (kg/m^3)	2,500
Young's modulus (Pa)	10^8
Poisson ratio	0.25
Coefficient of restitution	0.97
Friction between grains and inner wall	0.3
μ_{gw}	
Friction between grains μ_{gg}	0.3
Friction between grains and end-plates	0.3
μ_{gw}	
Timestep (s)	10^{-6}
Time period of rotation (s)	2
Dimensions of Cylinder (m)	$l = 0.14$ and $R = 0.14$

TABLE 3.3: Properties used for all non-spherical particle simulations

3.3.1 Prolate - prolate

Prolate is a spheroid in which one of the length of its principal axis is larger than the other two (which are equal). The shape of a prolate particle resembles that to a rugby ball. The shape is elongated and rod-like. To understand the segregation in a prolate-prolate mixture, two types of prolate particles with same aspect ratio were taken. Along each axis, the dimensions of the larger particle were twice that of the smaller one which makes the former eight times heavier than the latter. Exact dimension of each particle type are summarized in table 3.4.

Shapex, Shapey, Shapez (mm)	Mass fraction of each grain respectively
3, 6, 3 and 6, 12, 6	0.5 and 0.5

TABLE 3.4: Properties used for prolate-prolate mixture

3.3.2 Oblate - Oblate

It's an oblate spheroid that bulges at the equator and is somewhat squashed at the poles. The shape of the earth resemble to an oblate. It is a flattened spheroid, shaped like a lentil. Again, same aspect ratio was taken for both particles used in the simulation. Mass of the larger was eight times the mass of the smaller one. Exact dimension of each particle type are summarized in table 3.5.

Shapex, Shapey, Shapez (mm)	Mass fraction of each grain respectively
6, 1.5, 6 and 12, 3, 12	0.5 and 0.5

TABLE 3.5: Properties used for oblate-oblate mixture

Shapex, Shapey, Shapez (mm)	Mass fraction of each grain respectively
3, 6, 3 and 12, 3, 12	0.25 and 0.75

TABLE 3.6: Properties used for small prolate-big oblate mixture

3.3.3 Small Prolate - Big Oblate

3.3.4 Small Oblate - Big Prolate

Shapex, Shapey, Shapez (mm)	Mass fraction of each grain respectively
6, 1.5, 6 and 6, 12, 6	0.25 and 0.75

TABLE 3.7: Properties used for small oblate-big prolate

Chapter 4

Results and Discussion

4.1 Run A: Radial segregation for binary mixture of spherical particles

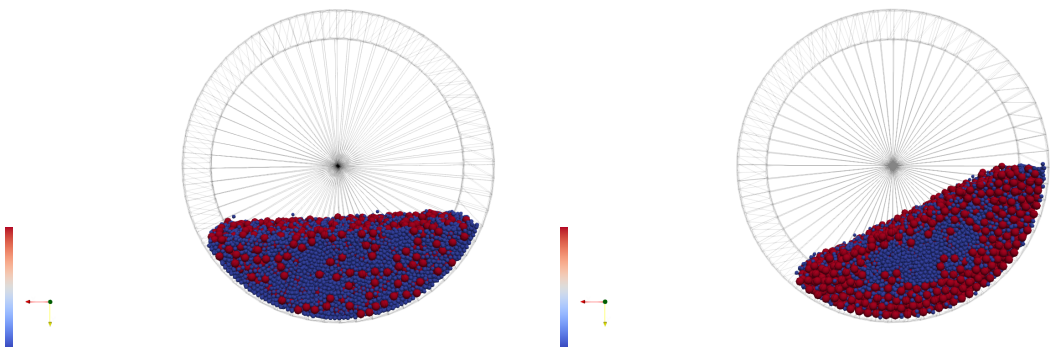


FIGURE 4.1: Radial view of simulation at $t = 1$ s and at $t = 20$ s

The figure 4.1 are the screenshots of the simulation at initial time and after 20 s. Initially, particles of different radii were present randomly inside the cylinder. After rotating the cylinder, a core of smaller particles was formed which is referred to as radial segregation. Radial segregation appears very early in the run and a core of small particles persists throughout the simulation.

4.2 Run B: Axial segregation for binary mixture of spherical particles

Since the two axially segregated particles differed only in size, it can be safely concluded that this type of segregation is possible when there is a difference only in the size. In order to measure the degree of axial segregation, the following definition is employed:

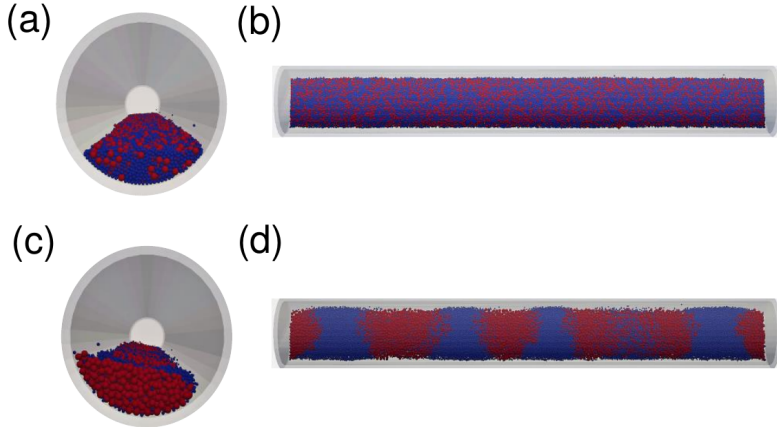


FIGURE 4.2: (a) and (b) are initial state while (c) and (d) are the state of the system after 125 rotations. In the final state, bands are pure with no radial core of small particles.

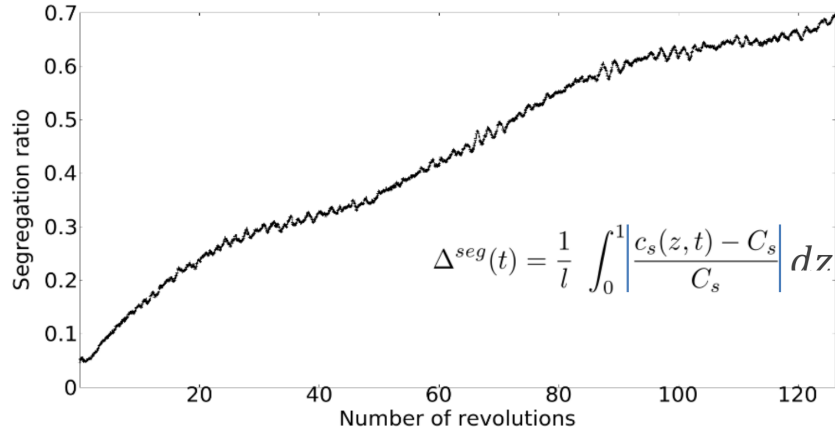


FIGURE 4.3: Segregation ratio is plotted against cylinder revolutions. Segregation ratio is defined such that for pure axial band, it becomes 1 and for a completely mixed state, its value is 0.

$$\Delta^{seg}(t) = \frac{1}{l} \int_0^1 \left| \frac{c_s(z, t) - C_s}{C_s} \right| dz \quad (4.1)$$

In the above equation the concentration (number of particles per unit length) of smaller are represented by $c_s(z, t)$ and the average concentration of smaller particles along the axial length is represented by $C_s = N_s/l$. This definition of segregation ratio would be equal to zero when the two types of particles are uniformly mixed. Moreover, the definition would yield 1 if pure bands of each type of particle are formed along the axial direction. See Fig. 4.3 for the plot of Δ^{seg} vs simulation time. The degree of segregation increases steadily in our case indicating that longer simulation runs are required to get more insight.

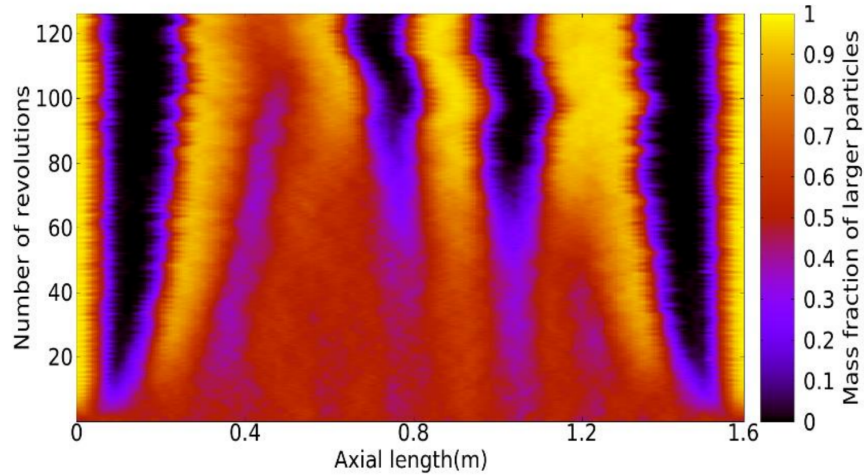


FIGURE 4.4: Space time plot representing mass fraction of large particles along the axial length.

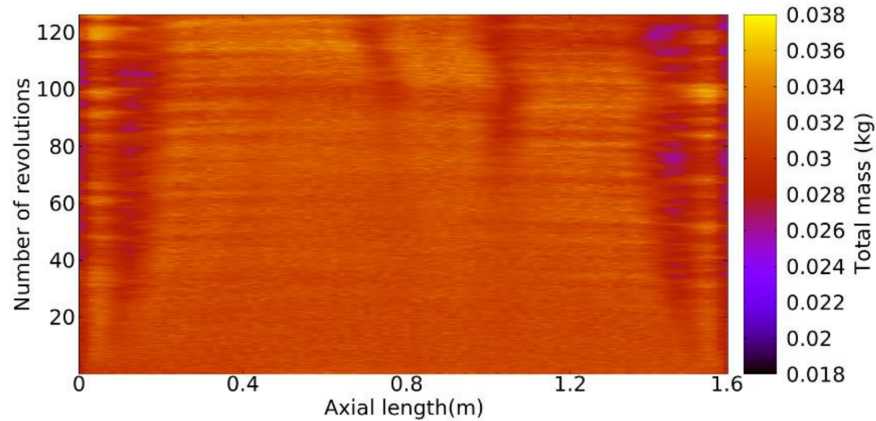


FIGURE 4.5: Space time plot depicting total mass variation along axial length and with time.

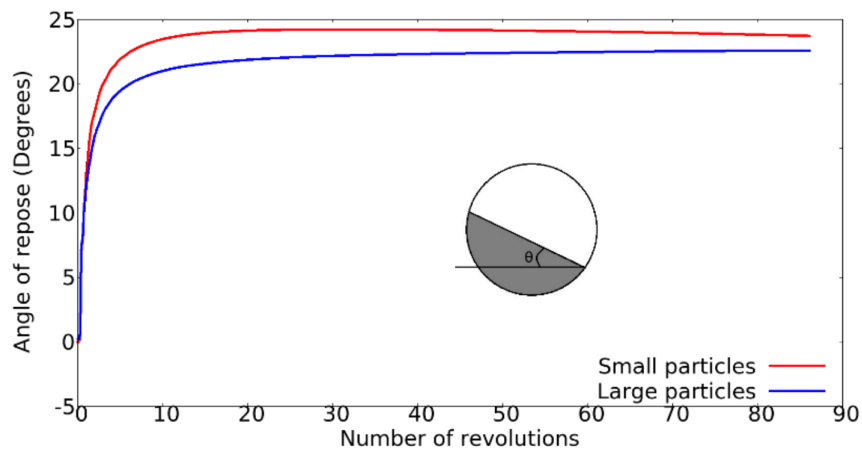


FIGURE 4.6: Graph of angle of repose of the bed vs simulation time, plotted for both particles of different radii.

The space-time plots (fig. 4.4 and fig. 4.5) shows how the segregation phenomena is changing along the spatial and with respect to time axis. These plots were obtained by dividing the cylinder into 100 equal parts along the axial length and finding the number of both type of particle in each of these parts for every time step. The so-generated data was plotted to generate such space-time plots. The particles are redistributed according to their sizes and are segregating into axial bands. A similar redistribution for total mass was not found. This is clear from the fig. 4.5 as the color of the space-time is constant along the axial length. We also observe that the bands are not symmetrical in the axial direction which is odd and counterintuitive. It is also evident that evolution of axial bands occurred at time scales that were too large that required to observe radial segregation.

Fig. 4.6 show the resultant angle of free surface for each type of particle inside the cylinder as a function of simulation time. For both the particles, the angle of repose increases with the number of rotations completed by the cylinder. More importantly, the difference between the angle of repose for different particles depends upon the number of rotation completed. Furthermore, this simulation study indicates that the angle of repose for the two particles should be different for axial segregation to take place.

4.3 Run C: Segregation in Non-spherical particle mixture

The segregation is measured by using the following definition:

$$\Delta^{seg} = \frac{1}{A} \int_r \int_\theta \frac{|c(r, \theta) - \gamma C(r, \theta)|}{c(r, \theta + \gamma C(r, \theta))} r dr d\theta \quad (4.2)$$

where $c(r, \theta)$ and $C(r, \theta)$ are defined as the number of smaller and larger particles per unit area respectively. γ is the ratio of number of smaller to larger particles. A is the cross sectional area of the cylinder filled with particles. r and θ are the polar coordinates.

This definition of segregation ratio gives a value of 0 when the two types of particles are well mixed. It gives a value of 1 when the system of particles are completely segregated. This definition of segregation ratio is used in Fig. 4.7 to produce plots for different granular mixtures. It is clear that the segregation is clearly happening for a mixture of small prolate particles with the bigger oblate particles as is indicated by an increase in the segregation ratio with respect to time (see Fig. 4.7). It is also interesting to note that for prolate-prolate mixture, the segregation ratio is higher than that for oblate-oblate mixture. Although, initial values of segregation ratio is higher for prolate-prolate mixture as compared to oblate-oblate, the larger value of slope for the former graph also indicates that segregation in prolate-prolate mixture is more prominent than oblate-oblate mixture.

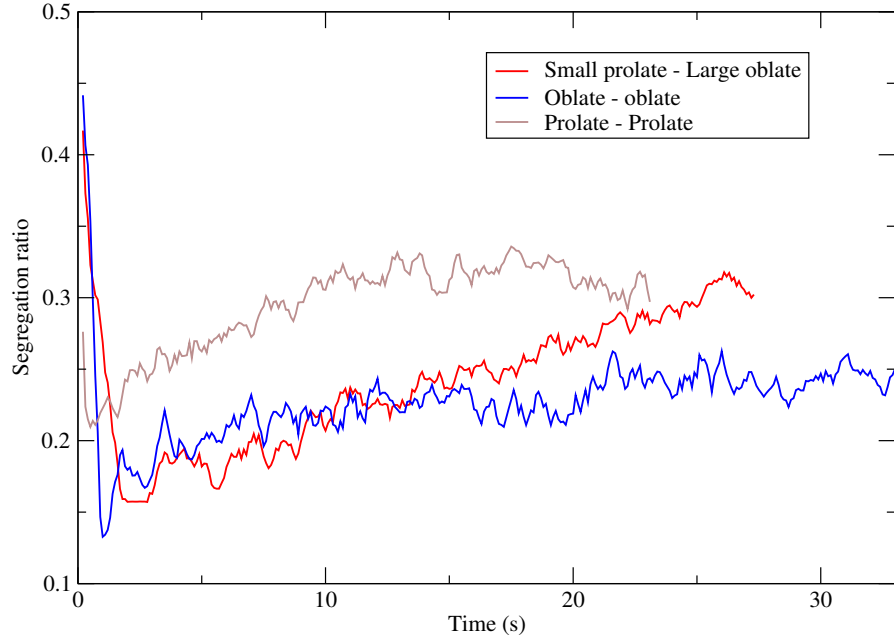


FIGURE 4.7: Segregation ratio for granular mixtures plotted against simulation time.

4.3.1 Prolate-prolate Mixture

One of the most interesting feature about the prolate particles is its tendency to form a relatively higher packing fraction than other shapes. They are rod-like and elongated structures.

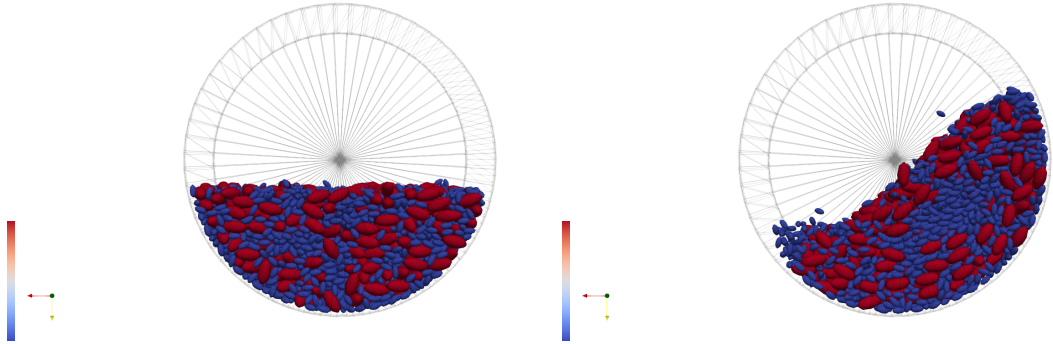


FIGURE 4.8: Prolate-prolate: Initial and final snapshot at $t = 1$ s and $t = 34$ s respectively.

After rotating the cylinder for a certain time filled with a mixture of smaller and larger prolate particles, we observe that smaller particles are grouping together and accumulating near the center of the cylinder (See Fig. 4.8). This result is similar to one observed in case of a spherical particle mixture (see Fig. 4.1). The evolution of radial core of small particles is depicted in Fig. 4.9. It can be seen that the concentration (number of particles per unit area) of smaller particles near the core ($r = 0.64 R$) is increasing while away from the core ($r = R$) the concentration is decreasing with time. Opposite is true

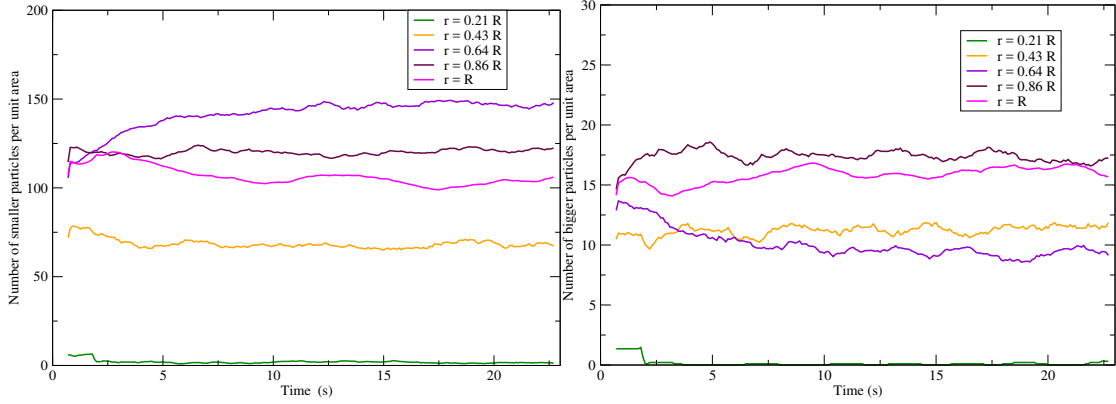


FIGURE 4.9: Prolate-prolate: Concentration vs simulation time for smaller and larger particles respectively

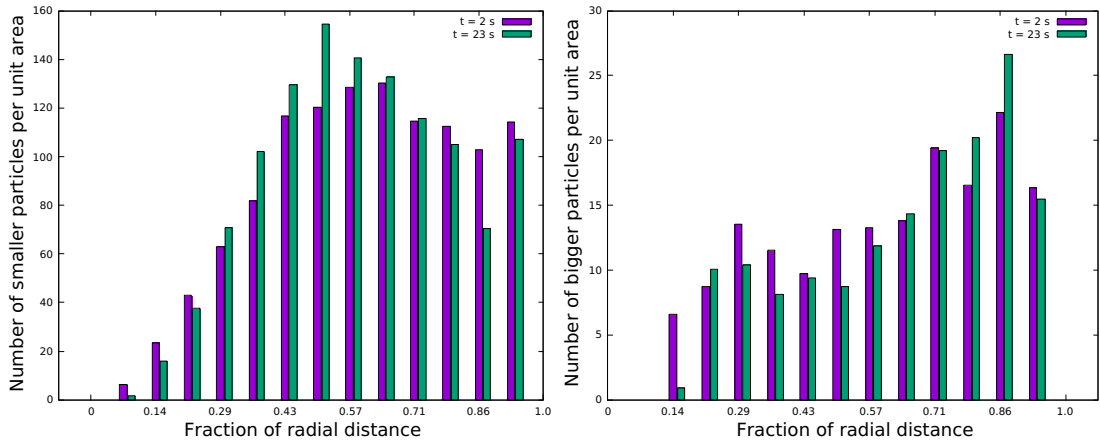


FIGURE 4.10: Prolate-prolate: Distribution of smaller and larger particles in the radial direction repectively

for larger particles (see Fig. 4.9 (b)). Particle distribution along the radial direction is shown in Fig. 4.10 for initial and final instant of the simulation. From the figure it can be inferred that the for number of smaller prolates are increasing in the region near $r = 0.5 R$ and decreasing near the wall. However, for the larger prolate particles, count is decreasing near $r = 0.5 R$ and increasing near the wall. Hence, it can be concluded evidently that the smaller particles are migrating towards the core of the cylinder and the larger particles are getting grouped near the walls. This shows that the prolate-prolate mixture is getting radially segregated based on their size.

4.3.2 Oblate-oblate Mixture

Fig. 4.11 shows the radial view of simulation during the rotation of horizontal drum at different instants. The radial core of small oblate particles cannot be clearly distinguished using this figure. From fig. 4.12 (a) it can be seen that the concentration of small oblate particles is not varying at any radial distance. This is evident as the segregation ratio is also not increasing for this granular mixture. Same is true for bigger oblate

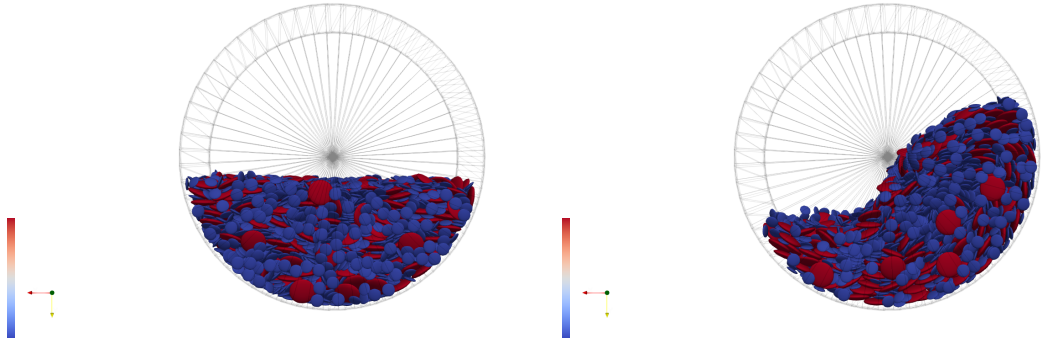


FIGURE 4.11: Oblate-oblate: Initial and final snapshot at $t = 1$ s and $t = 34$ s respectively.

particles. Slight increase in the concentration of smaller oblate particles is seen near $r = 0.5 R$ (see fig. 4.13 followed by a slight decrease near the walls. For larger particles the concentration is reduced sparingly near $r = 0.3 R$. Therefore, proofs of only partial segregation can be seen for oblate-oblate mixture. The higher value of segregation ratio for prolate-prolate mixute than oblate-oblate mixture shows the higher percolation tendency of prolates as compared to oblates of same volume and mass.

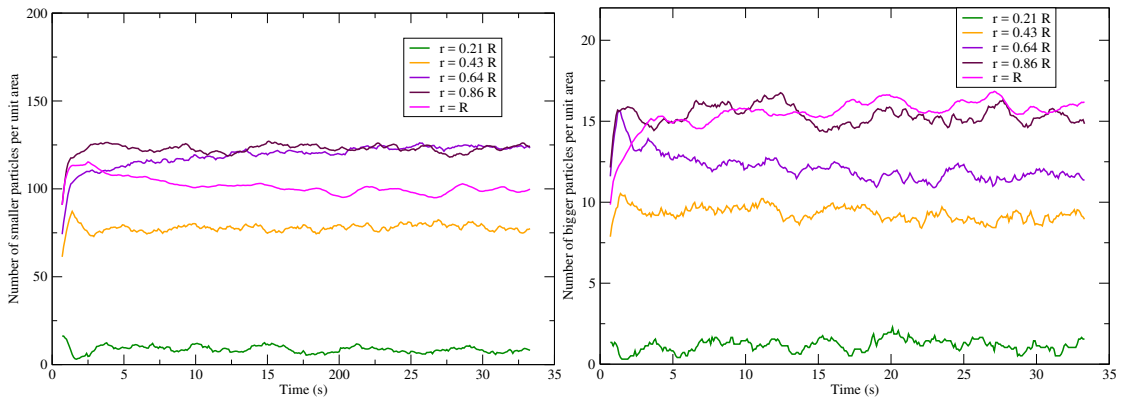


FIGURE 4.12: Oblate-oblate: Concentration vs simulation time for smaller and larger particles respectively

4.3.3 Small-prolate Big-oblate Mixture

Fig. 4.14 shows the evolution of mixed prolate-oblate mixture to a segregated one. The radial core of smaller prolate particles near the center of the cylinder can be clearly seen. To confirm this observation, 4.16 shows the variation in the concentration of both particles as a function of simulation time. It can be affirmed that the concentration of smaller prolate particles is incresing near the core ($r = 0$), decreasing near the walls ($r = R$) and is constant between them. Larger particles are migrating away from the core as can be seen from fig. 4.14 (b) and concentration near the walls. Fig. 4.16 shows the concentration of small particles near the core has almost double within few revolution

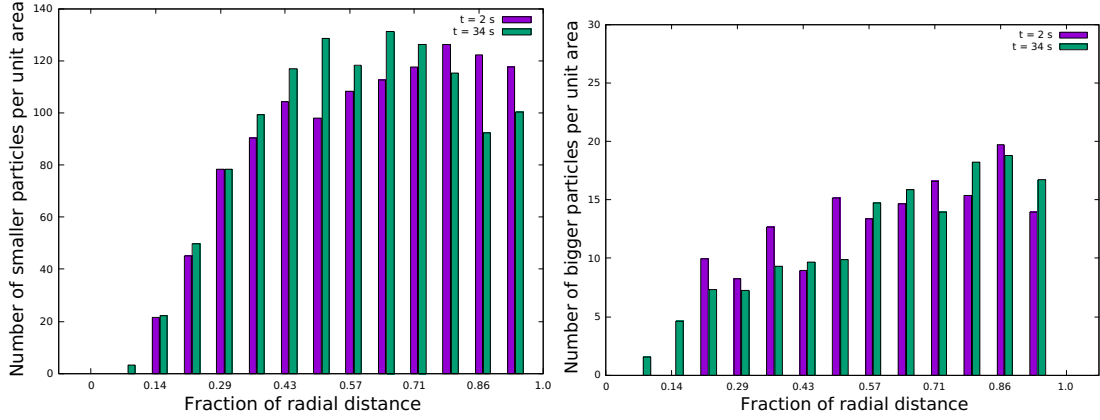


FIGURE 4.13: Oblate-oblate: Distribution of smaller and larger particles in the radial direction repectively

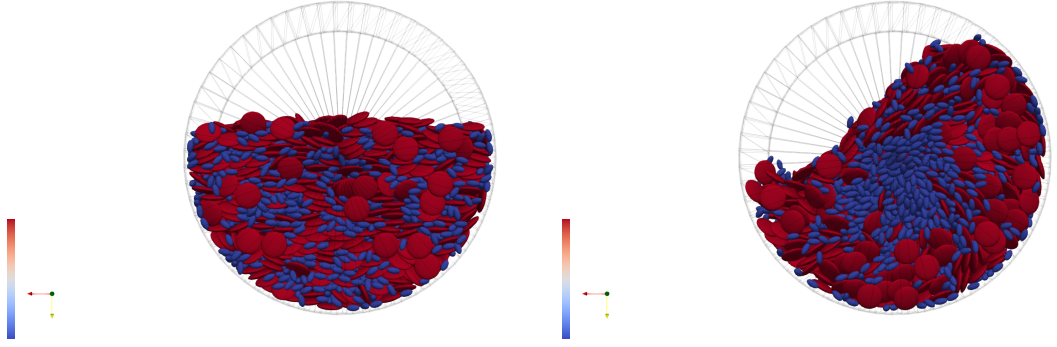


FIGURE 4.14: Small prolate - large oblate: Initial and final snapshot at $t = 2\text{ s}$ and $t = 35\text{ s}$ respectively.

of the cylinder. On the other hand, the decrease in the concentration of larger oblate particles can also be seen near the center of the cylinder.

One can also see that in fig. 4.15 the fluctuations in the graph are larger for $r = 0$ and smaller for $r = R$. From this interesting observation it can be inferred that near the core the particles are moving at higher velocities while the particles near the walls are moving through a smooth streamline.

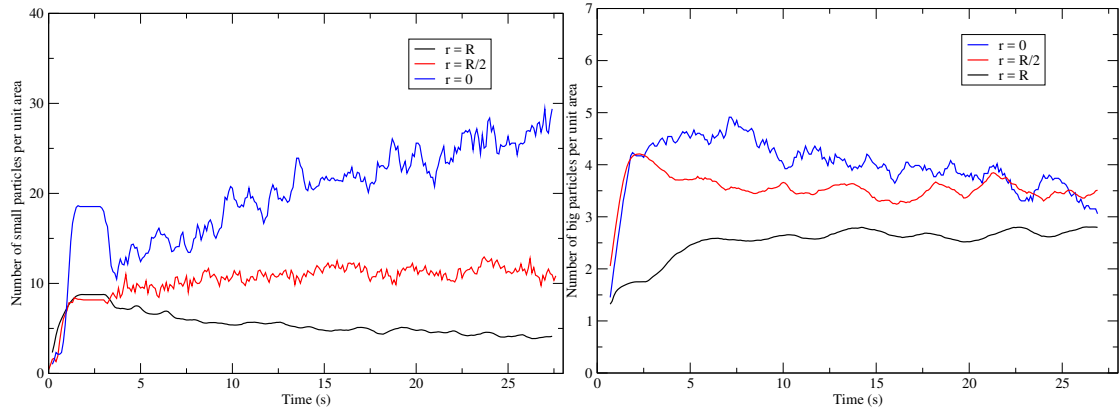


FIGURE 4.15: Small prolate - large oblate: Concentration vs simulation time for smaller and larger particles respectively

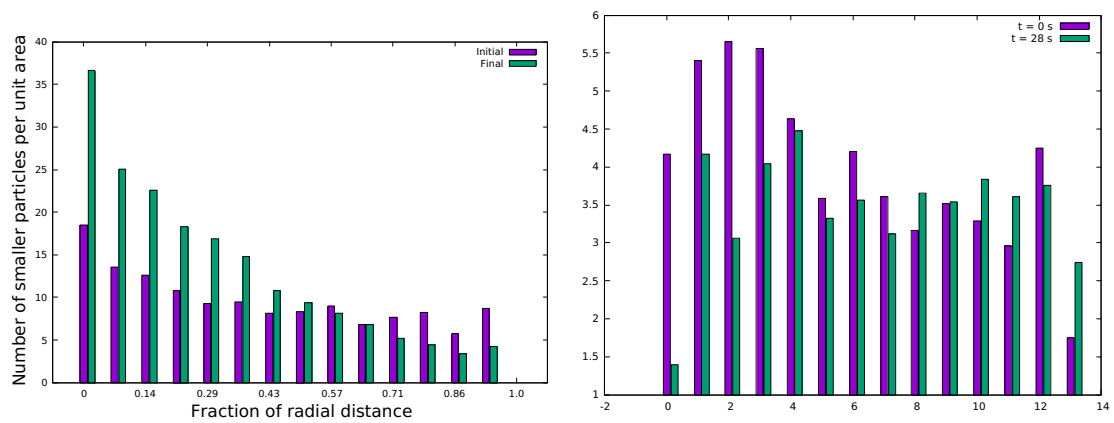


FIGURE 4.16: Small prolate - large oblate: Distribution of smaller and larger particles in the radial direction repectively

Chapter 5

Conclusions

We have found that discrete element method employed in this thesis to study granular dynamics is suitable and accurate. It is possible to get more insights from these simulations than from doing experiments alone. We were able to point out partially the fundamental mechanisms behind different particle segregation. We have demonstrated size segregation for spherical particles. To investigate more on the effect of side plates, longer cylinders were used. Then we have described and presented axial segregation for spherical particles. We defined segregation ratio and plotted its variation with the number of revolutions completed by cylinder. Then we focussed on understanding the time evolution of axial band formation. We also plotted the angle of repose for each type of particle and found that the angle difference was 2-3 deg which should be sufficient to produce axial segregation. Since density of both the particles and friction coefficient between them and wall were same, our simulation shows that frictional properties need not be different for axial segregation to take place. For Non-spherical particles, we made an attempt to understand the conditions under which radial segregation takes place. We took different particle mixture and plotted their segregation ratio against simulation time. We also showed the evolution of the radial core for all particle mixtures. Despite taking these steps, it was not possible for us to explain all the segregation phenomena observed for non-spherical particles.

It could therefore be concluded that granular dynamics is still mysterious and various phenomena are still not clear from understanding point of view. Therefore, more research work needs to be done before declaring this field as mature.

5.1 Outlook

The radial segregation for spherical particles is relatively well understood. End walls were shown to have strong influence on formation of axial bands. The difference in the angle of repose was confirmed between the particles that were axially segregated. The

reason for this is not yet clear and would require further research. The preference the large particles impose to segregate at the end walls is not clearly understood although several attempts have been made. For non-spherical particles, the reason behind larger segregation ratio for prolate-prolate mixture as compared to oblate-oblate mixture remains unknown. So far, researchers have been able to explain size-based segregation, but in our case, segregation is happening because of different particle shape as well. Therefore, the mechanisms behind all the segregation phenomena for different particle shapes and sizes should be further studied.

Bibliography

- [1] Shiliang Yang, Liangqi Zhang, Kun Luo, and Jia Wei Chew. Dem study of the size-induced segregation dynamics of a ternary-size granular mixture in the rolling-regime rotating drum. *Physics of Fluids*, 29(12):123301, 2017. doi: 10.1063/1.5008297. URL <https://doi.org/10.1063/1.5008297>.
- [2] Bhateja A. Scaling of granular temperature in vibro-fluidized grains. *Phys. Fluids*, 28:043301, 2016.
- [3] Kumawat T. C. Stability analysis of the rimming flow inside a uniformly heated rotating horizontal cylinder. *Phys. Fluids*, 29:032102, 2017.
- [4] Gray J. M. N. T. Granular flow in partially filled slowly rotating drums. *J. Fluid Mech.*, 441:1, 2001.
- [5] Mellmann J. The transverse motion of solids in rotating cylindersforms of motion and transition behavior. *Powder Technol.*, 118:251, 2001.
- [6] Dahl S. R. Size segregation in rapid, granular flows with continuous size distributions. *Phys. Fluids*, 16:1, 2004.
- [7] Dury C. M. Competition of mixing and segregation in rotating cylinders. *Phys. Fluids*, 11:1387, 1999.
- [8] Zuriguel I. Pattern selection by a granular wave in a rotating drum. *Phys. Rev. E*, 73:061302, 2006.
- [9] Huang A. N. A study of the three-dimensional particle size segregation structure in a rotating drum. *AICHE J.*, 58:1076, 2012.
- [10] Windows-Yule C. Understanding and exploiting competing segregation mechanisms in horizontally rotated granular media. *New J. Phys.*, 18:023013, 2016.
- [11] Tilo F. A. M. S. The mechanism of long-term coarsening of granular mixtures in rotating drums. *New J. Phys.*, 17:093023, 2015.
- [12] Mandal S. A study of the rheology of planar granular flow of dumbbells using discrete element method simulations. *Phys. Fluids*, 28:103301, 2016.

- [13] Richard P. Recent advances in dem simulations of grains in a rotating drum. *Soft Matter*, 4:1345, 2008.
- [14] Yang R. Y. Numerical simulation of particle dynamics in different flow regimes in a rotating drum. *Powder Technol.*, 188:170, 2008.
- [15] Finnie G. J. Longitudinal and transverse mixing in rotary kilns: A discrete element method approach. *Chem. Eng. Sci.*, 60:4083, 2005.
- [16] Rapaport D. C. Radial and axial segregation of granular matter in a rotating cylinder: A simulation study. *Phys. Rev. E*, 75:031301, 2007.
- [17] Chen P. Subsurface granular flow in rotating tumblers: A detailed computational study. *Phys. Rev. E*, 78:021303, 2008.
- [18] Yang S. Segregation dynamics of a binary-size mixture in a three-dimensional rotating drum. *Chem. Eng. Sci.*, 172:652, 2017.
- [19] Newey M. Band-in-band segregation of multidisperse granular mixtures. *Europhys. Lett.*, 66:205, 2004.
- [20] Shimokawa M. Pattern formation in a sandpile of ternary granular mixtures. *Phys. Rev. E*, 91:062205, 2015.
- [21] Hajra S. K. Radial segregation of ternary granular mixtures in rotating cylinders. *Granular Matter*, 13:475, 2011.
- [22] Pereira G. G. Radial segregation of multi-component granular media in a rotating tumbler. *Granular Matter*, 15:705, 2013.
- [23] Alizadeh E. Characterization of mixing and size segregation in a rotating drum by a particle tracking method. *AIChe J.*, 59:1894, 2013.
- [24] Cundall P. A. A discrete numerical model for granular assemblies. *Geotechnique*, 29:47, 1979.
- [25] Ai J. Assessment of rolling resistance models in discrete element simulations. *Powder Technol.*, 206:269, 2011.
- [26] Yang S. Particle-scale investigation of the solid dispersion and residence properties in a 3-d spout-fluid bed. *AIChe J.*, 60:2788, 2014.
- [27] Yang S. Dem study of granular flow characteristics in the active and passive regions of a three-dimensional rotating drum. *AIChe J.*, 62:3874, 2016.
- [28] Gray J. M. N. T. Multi-component particle-size segregation in shallow granular avalanches. *J. Fluid Mech.*, 678:535, 2011.
- [29] Hill K. M. Reversible axial segregation of rotating granular media. *Phys. Rev. E*, 52:4393, 1995.

- [30] Rasouli M. Investigating the dynamics of cylindrical particles in a rotating drum using multiple radioactive particle tracking. *AIChE J.*, 62:2622, 2016.
- [31] Ding Y. L. Granular motion in rotating drums: Bed turnover time and slumping-rolling transition. *Powder Technol.*, 124:18, 2002.
- [32] Yang S. Impact of granular segregation on the solid residence time and active-passive exchange in a rotating drum. *Chem. Eng. Sci.*, 173:287, 2017.
- [33] Christov I. C. Resolving a paradox of anomalous scalings in the diffusion of granular materials. *Proc. Natl. Acad. Sci. U. S. A.*, 109:16012, 2012.